Biomedical Optics EXPRESS

Effect of temperature and fixation on the optical properties of atherosclerotic tissue: a validation study of an ex-vivo whole heart cadaveric model

Muthukaruppan Gnanadesigan,[1,*] Gijs van Soest,[1] Stephen White,[2] Simon Scoltock,[2] Giovanni J Ughi,[4] Andreas Baumbach,[2] Antonius FW van der Steen,[1,3] Evelyn Regar,[1] and Thomas W Johnson[2]

[1]*Department of Biomedical Engineering, Erasmus Medical Center, PO Box 2040, 3000 CA Rotterdam, The Netherlands*

[2]*Bristol Heart Institute, Bristol, UK*

[3] *Department of Imaging Science and Technology, Delft University of Technology, Lorentzweg 1, 2628 CJ Delft, The Netherlands*

[4]*Cardiovascular Diseases, University Hospitals Leuven, & Dept. of Cardiovascular Sciences, KU Leuven, Belgium*

**m.gnanadesigan@erasmusmc.nl*

Abstract: Atherosclerotic plaque composition can be imaged using the optical attenuation coefficient derived from intravascular optical coherence tomography (OCT) data. The relation between optical properties and tissue type has been established on autopsy tissues. In this study, we validate an ex-vivo model for the effect of temperature and tissue fixation on optical parameters. We studied the optical attenuation of human coronary arteries at three temperatures, before and after formalin fixation. We developed an en-face longitudinal display of attenuation data of the OCT pullbacks. Using the unfixed, body-temperature condition image as a standard, and after extensive registration with other condition images, we quantify the differences in optical attenuation and the backscattered intensity. The results suggest that tissue fixation and temperature do not introduce systematic errors in studies of arterial optical properties.

OCIS codes: (170.4500) Optical coherence tomography; (170.3880) Medical and biological imaging; (170.3010) Image reconstruction techniques; (110.2960) Image analysis.

References and links

1. E. Falk, P. K. Shah, and V. Fuster, "Coronary Plaque Disruption," Circulation **92**(3), 657–671 (1995).
2. J. A. Schaar, J. E. Muller, E. Falk, R. Virmani, V. Fuster, P. W. Serruys, A. Colombo, C. Stefanadis, S. Ward Casscells, P. R. Moreno, A. Maseri, and A. F. van der Steen, "Terminology for high-risk and vulnerable coronary artery plaques," Eur. Heart J. **25**(12), 1077–1082 (2004).
3. R. Virmani, F. D. Kolodgie, A. P. Burke, A. Farb, and S. M. Schwartz, "Lessons from sudden coronary death: A comprehensive morphological classification scheme for atherosclerotic lesions," Arterioscler. Thromb. Vasc. Biol. **20**(5), 1262–1275 (2000).
4. S. Waxman, M. I. Freilich, M. J. Suter, M. Shishkov, S. Bilazarian, R. Virmani, B. E. Bouma, and G. J. Tearney, "A case of lipid core plaque progression and rupture at the edge of a coronary stent: Elucidating the mechanisms of drug-eluting stent failure," Circ. Cardiovasc. Interv. **3**(2), 193–196 (2010).
5. J. A. Goldstein, C. Grines, T. Fischell, R. Virmani, D. Rizik, J. Muller, and S. R. Dixon, "Coronary Embolization Following Balloon Dilation of Lipid-Core Plaques," JACC Cardiovasc. Imaging **2**(12), 1420–1424 (2009).
6. A. Tanaka, T. Imanishi, H. Kitabata, T. Kubo, S. Takarada, T. Tanimoto, A. Kuroi, H. Tsujioka, H. Ikejima, K. Komukai, H. Kataiwa, K. Okouchi, M. Kashiwaghi, K. Ishibashi, H. Matsumoto, K. Takemoto, N. Nakamura, K. Hirata, M. Mizukoshi, and T. Akasaka, "Lipid-rich plaque and myocardial perfusion after successful stenting in patients with non-ST-segment elevation acute coronary syndrome: an optical coherence tomography study," Eur. Heart J. **30**(11), 1348–1355 (2009).
7. E. Regar, J. Ligthart, N. Bruining, and G. van Soest, "The diagnostic value of intracoronary optical coherence tomography," Herz **36**(5), 417–429 (2011).
8. G. J. Tearney, E. Regar, T. Akasaka, T. Adriaenssens, P. Barlis, H. G. Bezerra, B. Bouma, N. Bruining, J. M. Cho, S. Chowdhary, M. A. Costa, R. de Silva, J. Dijkstra, C. Di Mario, D. Dudek, E. Falk, M. D. Feldman, P.

#202313 - $15.00 USD Received 5 Dec 2013; revised 24 Jan 2014; accepted 1 Feb 2014; published 3 Mar 2014

Fitzgerald, H. M. Garcia-Garcia, N. Gonzalo, J. F. Granada, G. Guagliumi, N. R. Holm, Y. Honda, F. Ikeno, M. Kawasaki, J. Kochman, L. Koltowski, T. Kubo, T. Kume, H. Kyono, C. C. S. Lam, G. Lamouche, D. P. Lee, M. B. Leon, A. Maehara, O. Manfrini, G. S. Mintz, K. Mizuno, M. A. Morel, S. Nadkarni, H. Okura, H. Otake, A. Pietrasik, F. Prati, L. Räber, M. D. Radu, J. Rieber, M. Riga, A. Rollins, M. Rosenberg, V. Sirbu, P. W. J. C. Serruys, K. Shimada, T. Shinke, J. Shite, E. Siegel, S. Sonoda, M. Suter, S. Takarada, A. Tanaka, M. Terashima, T. Thim, S. Uemura, G. J. Ughi, H. M. M. van Beusekom, A. F. W. van der Steen, G.-A. van Es, G. van Soest, R. Virmani, S. Waxman, N. J. Weissman, and G. Weisz; International Working Group for Intravascular Optical Coherence Tomography (IWG-IVOCT), "Consensus Standards for Acquisition, Measurement, and Reporting of Intravascular Optical Coherence Tomography Studies: A Report From the International Working Group for Intravascular Optical Coherence Tomography Standardization and Validation," J. Am. Coll. Cardiol. **59**(12), 1058–1072 (2012).

9. G. Guagliumi, M. A. Costa, V. Sirbu, G. Musumeci, H. G. Bezerra, N. Suzuki, A. Matiashvili, N. Lortkipanidze, L. Mihalcsik, A. Trivisonno, O. Valsecchi, G. S. Mintz, O. Dressler, H. Parise, A. Maehara, E. Cristea, A. J. Lansky, R. Mehran, and G. W. Stone, "Strut Coverage and Late Malapposition With Paclitaxel-Eluting Stents Compared With Bare Metal Stents in Acute Myocardial Infarction: Optical Coherence Tomography Substudy of the Harmonizing Outcomes With Revascularization and Stents in Acute Myocardial Infarction (HORIZONS-AMI) Trial," Circulation **123**(3), 274–281 (2011).
10. G. Guagliumi, G. Musumeci, V. Sirbu, H. G. Bezerra, N. Suzuki, L. Fiocca, A. Matiashvili, N. Lortkipanidze, A. Trivisonno, O. Valsecchi, G. Biondi-Zoccai, and M. A. Costa; ODESSA Trial Investigators, "Optical Coherence Tomography Assessment of In Vivo Vascular Response After Implantation of Overlapping Bare-Metal and Drug-Eluting Stents," JACC Cardiovasc. Interv. **3**(5), 531–539 (2010).
11. H. Yabushita, B. E. Bouma, S. L. Houser, H. T. Aretz, I. K. Jang, K. H. Schlendorf, C. R. Kauffman, M. Shishkov, D. H. Kang, E. F. Halpern, and G. J. Tearney, "Characterization of human atherosclerosis by optical coherence tomography," Circulation **106**(13), 1640–1645 (2002).
12. T. Kume, T. Akasaka, T. Kawamoto, N. Watanabe, E. Toyota, Y. Neishi, R. Sukmawan, Y. Sadahira, and K. Yoshida, "Assessment of coronary arterial plaque by optical coherence tomography," Am. J. Cardiol. **97**(8), 1172–1175 (2006).
13. D. Levitz, L. Thrane, M. H. Frosz, P. E. Andersen, C. B. Andersen, S. Andersson-Engels, J. Valanciunaite, J. Swartling, and P. R. Hansen, "Determination of optical scattering properties of highly-scattering media in optical coherence tomography images," Opt. Express **12**(2), 249–259 (2004).
14. F. J. van der Meer, D. J. Faber, D. M. Baraznji Sassoon, M. C. Aalders, G. Pasterkamp, and T. G. van Leeuwen, "Localized measurement of optical attenuation coefficients of atherosclerotic plaque constituents by quantitative optical coherence tomography," IEEE Trans. Med. Imaging **24**(10), 1369–1376 (2005).
15. G. van Soest, T. Goderie, E. Regar, S. Koljenović, G. L. van Leenders, N. Gonzalo, S. van Noorden, T. Okamura, B. E. Bouma, G. J. Tearney, J. W. Oosterhuis, P. W. Serruys, and A. F. van der Steen, "Atherosclerotic tissue characterization in vivo by optical coherence tomography attenuation imaging," J. Biomed. Opt. **15**(1), 011105 (2010).
16. E. Regar, M. Gnanadesigan, A. F. W. Van der Steen, and G. van Soest, "Quantitative Optical Coherence Tomography Tissue-Type Imaging for Lipid-Core Plaque Detection," JACC Cardiovasc. Interv. **6**(8), 891–892 (2013).
17. G. J. Ughi, T. Adriaenssens, P. Sinnaeve, W. Desmet, and J. D'hooge, "Automated tissue characterization of in vivo atherosclerotic plaques by intravascular optical coherence tomography images," Biomed. Opt. Express **4**(7), 1014–1030 (2013).
18. J. C. Bamber, M. J. Fry, C. R. Hill, and F. Dunn, "Ultrasonic attenuation and backscattering by mammalian organs as a function of time after excision," Ultrasound Med. Biol. **3**(1), 15–20 (1977).
19. J. C. Bamber and C. R. Hill, "Ultrasonic attenuation and propagation speed in mammalian tissues as a function of temperature," Ultrasound Med. Biol. **5**(2), 149–157 (1979).
20. J. C. Bamber, C. R. Hill, J. A. King, and F. Dunn, "Ultrasonic propagation through fixed and unfixed tissues," Ultrasound Med. Biol. **5**(2), 159–165 (1979).
21. Schaar, J. A., C. L. de Korte, F. Mastik and A. F. van der Steen, "Effect of temperature increase and freezing on intravascular elastography," Ultrasonics **40**(1–8), 879–881 (2002).
22. A. F. van der Steen, M. H. Cuypers, J. M. Thijssen, and P. C. de Wilde, "Influence of histochemical preparation on acoustic parameters of liver tissue: a 5-MHz study," Ultrasound Med. Biol. **17**(9), 879–891 (1991).
23. A. F. van der Steen, J. M. Thijssen, G. P. Ebben, and P. C. de Wilde, "Effects of tissue processing techniques in acoustical (1.2 GHz) and light microscopy," Histochemistry **97**(2), 195–199 (1992).
24. M. Nakano, M. Vorpahl, F. Otsuka, M. Taniwaki, S. K. Yazdani, A. V. Finn, E. R. Ladich, F. D. Kolodgie, and R. Virmani, "Ex vivo assessment of vascular response to coronary stents by optical frequency domain imaging," JACC Cardiovasc. Imaging **5**(1), 71–82 (2012).
25. T. Wang, W. Wieser, G. Springeling, R. Beurskens, C. T. Lancee, T. Pfeiffer, A. F. van der Steen, R. Huber, and G. van Soest, "Intravascular optical coherence tomography imaging at 3200 frames per second," Opt. Lett. **38**(10), 1715–1717 (2013).
26. T. W. Johnson, S. White, M. Gnanadesigan, H. Bourenane, J. W. Strange, A. C. Newby, G. van Soest, and A. Baumbach, "An ex-vivo "whole human heart model" for the development of intravascular imaging," Heart **98**(Suppl 1), A15–A16 (2012).

#202313 - $15.00 USD Received 5 Dec 2013; revised 24 Jan 2014; accepted 1 Feb 2014; published 3 Mar 2014

27. T. G. van Leeuwen, D. J. Faber, and M. C. Aalders, "Measurement of the axial point spread function in scattering media using single-mode fiber-based optical coherence tomography," IEEE J. Sel. Top. Quantum Electron. **9**(2), 227–233 (2003).
28. G. J. Ughi, T. Adriaenssens, K. Onsea, P. Kayaert, C. Dubois, P. Sinnaeve, M. Coosemans, W. Desmet, and J. D'hooge, "Automatic segmentation of in-vivo intra-coronary optical coherence tomography images to assess stent strut apposition and coverage," Int. J. Cardiovasc. Imaging **28**(2), 229–241 (2012).
29. O. A. Meissner, J. Rieber, G. Babaryka, M. Oswald, S. Reim, U. Siebert, T. Redel, M. Reiser, and U. Mueller-Lisse, "Intravascular optical coherence tomography: comparison with histopathology in atherosclerotic peripheral artery specimens," J. Vasc. Interv. Radiol. **17**(2), 343–349 (2006).

1. Introduction

Ischemic heart disease is a major cause of death globally and rupture of vulnerable atherosclerotic plaques, precipitating myocardial infarction, is the largest contributor to the phenomenon [1]. A vulnerable plaque commonly consists of a lipid-rich necrotic core contained by a fragile layer of fibrous tissue that can be compromised by inflammation and mechanical forces [2]. Release of the necrotic material into the bloodstream may cause thrombus formation leading to a myocardial infarction. Hence, the tissue composition of the plaque is an important predictor of its vulnerability [3]. Likewise, the presence of a lipid-core in a plaque may have an adverse effect on outcome of coronary interventions [4–6]. Intravascular optical coherence tomography (OCT) is gaining widespread use in the interventional cardiology community for guidance of stent placement and optimization [7–10]. OCT facilitates high resolution imaging of the atherosclerotic plaque and tissue components can be distinguished to ascertain plaque composition [8, 11, 12]. The contrast of tissue types derives from differences in optical properties of the tissues in the artery wall, which can be quantified for tissue characterization in OCT images. The attenuation coefficient has been a popular metric to achieve this [13, 14]: necrotic core and inflammation, associated with plaque vulnerability, have high attenuation compared to fibrous and calcified tissues [15].This finding is currently being clinically validated and appears to be robust in vivo [16]. The analysis has recently been augmented with statistical image metrics to achieve better specificity [17].

Validation of tissue characterization requires comparison of the optical attenuation against histological analysis of atherosclerotic tissue specimens; currently this can only be achieved using ex-vivo models. For ease of processing and analysis ex-vivo specimens of atherosclerotic tissue are commonly dissected from the myocardium, fixed with formalin and kept at low temperature for preservation. The effects of such processing on the acoustic properties of tissue have been studied extensively [18–23]. The knowledge of effects of such processing on tissue optics in the artery wall however is very scarce [24]. In comparison with in-vivo assessment of optical attenuation, refrigeration and fixation of tissue may significantly alter the optical attenuation characteristics of lipid and cellular components of atherosclerotic plaque. Assessment of the impact of temperature and fixation on the optical attenuation of atherosclerotic tissue is necessary to validate our ex-vivo whole heart cadaveric model, thereby facilitating translation into the clinical arena.

The assessment of the effect of temperature and fixation on optical attenuation requires co-registration of multiple OCT attenuation data sets, across varying conditions. It is important to recognize that accurate co-registration of OCT images is limited by a number of factors. Firstly, the helical rotation of the imaging probe during an OCT pullback combined with a narrow lateral width of imaging results in longitudinal under-sampling [25]. Furthermore, non-uniform rotation of the catheter, catheter movement and anatomical distortion can lead to misalignment of data sets.

The aim of this study is to assess the effect of temperature and fixation on optical attenuation in an ex-vivo whole heart cadaveric model, thereby facilitating development of a novel method of intra-vascular OCT tissue characterization.

#202313 - $15.00 USD Received 5 Dec 2013; revised 24 Jan 2014; accepted 1 Feb 2014; published 3 Mar 2014

2. Materials and methods

2.1 Tissue handling and imaging procedure

The ex-vivo model we used consists of a whole heart cadaveric specimen obtained from the Valve Bank of West-England within 48 hrs from post-mortem and stored at or below 4°C [26]. The heart specimen was mounted in a set up as shown in Fig. 1. A short guide catheter was introduced into the right coronary artery and fixed in position with sutures. All tissues were handled in accordance with the local ethics regulations. The cadaveric specimen is held within a purpose-built Perspex container, with adaptors on both sides of the container's lid allowing connection of the guide catheter internally, and a Y-connector and pressure/injector manifold externally.

The OCT system used for imaging was a C7-XR with Dragonfly catheter (St. Jude Medical Inc. St. Paul, MN, USA). Pullback OCT imaging of one of the three major coronary arteries was performed at a pullback speed of 20 mm/s. The end of the guide catheter served as a reference point to relate the different pullback data sets longitudinally.

Three different temperature conditions were induced in the vessel by flushing with phosphate buffered saline (PBS) solution at 4°C, 20°C, and 37°C, resulting in tissue temperatures of 5-8°C (cold), 18-21°C (room temperature) and 35-37°C (body temperature). A needle-probe thermometer (Water resistant thermometer, Traceable®, VWR International, LLC) was inserted into the peri-adventitial tissue of the coronary artery and imaging was delayed until steady state temperature was achieved. During imaging, intracoronary pressure was maintained at 100 mmHg. OCT imaging was undertaken at these three temperatures. Subsequently, the tissues were pressure fixed with buffered formalin at 100 mmHg for 15 minutes, preserving vessel morphology, and typically 500ml of formalin was perfused into the heart, which was left in situ overnight at 4°C. The next day, a new temperature series was collected in the fixed tissue, creating a data set of 6 different conditions. A total of 6 coronary arteries were imaged for the study.

After imaging the formalin fixed series, the study vessel was excised from the heart, fixed for a further 24 hours, embedded in paraffin, and cut into 4-mm blocks. The end of the guide catheter served as a reference. The end face of each block is serially sectioned into slices of 3 μm thickness and stained for histologic analysis. In case of extensive disease seen on OCT, serial sections through the entire tissue block are generated. OCT data were matched to the histology cross-sections based on longitudinal position and general anatomy (side branches and presence of plaque).

In the description of the results in this paper we will adopt the following labels: data acquired on unfixed tissues will be designated by "U"; on fixed tissues by "F". The temperatures will be indicated by "C" for cold, "R" for room, and "B" for body temperature. For example, our base condition of unfixed tissue at 37°C will be referred to as "UB".

#202313 - $15.00 USD Received 5 Dec 2013; revised 24 Jan 2014; accepted 1 Feb 2014; published 3 Mar 2014

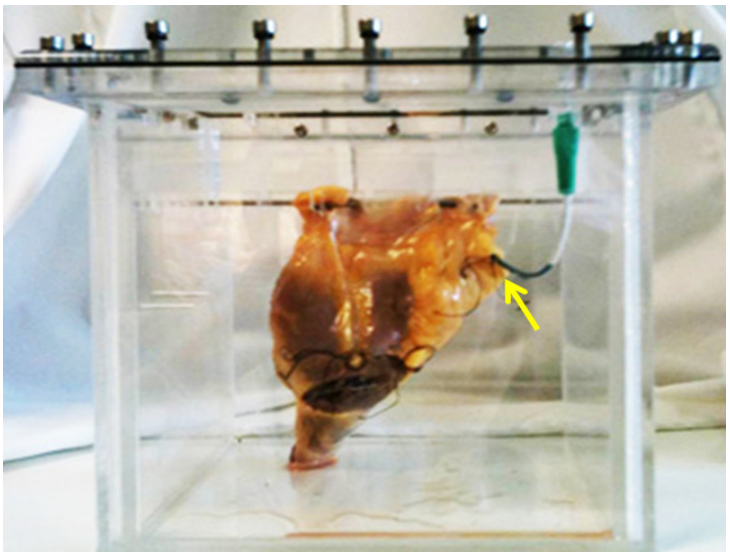

Fig. 1. Whole heart cadaveric model; the arrow points to the guide catheter that is fixed in the study vessel.

2.2 Parameter extraction

The OCT images are then analyzed, to quantify the attenuation exhibited by the tissues. We derive the attenuation co-efficient from the OCT signal by fitting a single scattering model [15]:

$$\langle I_d \rangle = T(r) \cdot \mathrm{S(r)} \cdot \mathrm{I}_0 \cdot e^{-\mu_t r} \qquad (1)$$

where T(r) is the point spread function of the catheter [27], S(r) is the signal roll-off, and the parameter of interest is μ_t, the attenuation coefficient. The attenuation calculation and the model implementation were done in Matlab Release 2012b (The Mathworks, Inc., Natick, MA, USA). The model is fitted in the polar image, in every A-line starting from the edge of the lumen [15,28], in small windows of varying length to extract the attenuation coefficients. The accuracy of the extracted μ_t is approximately 1 mm^{-1} [15]. The data analysis results in an attenuation image per cross section of the pullback.

2.3 Image formation and registration

In every vessel in the study, attenuation data sets are generated in six different conditions, resulting in six data sets that need to be registered for comparison. As a first step, the variation in the angle of view of a structure due to the different positioning of the catheter in different pullbacks should be compensated.

To do so, the polar attenuation image is converted to the Cartesian domain, the center of the image is shifted from the catheter to the centroid of the lumen, and the image is converted back to the polar domain relative to the new image center. Figure 2 depicts the OCT and the attenuation images with the lumen border, the centroid and the corresponding polar image before and after the origin shift.

#202313 - $15.00 USD Received 5 Dec 2013; revised 24 Jan 2014; accepted 1 Feb 2014; published 3 Mar 2014

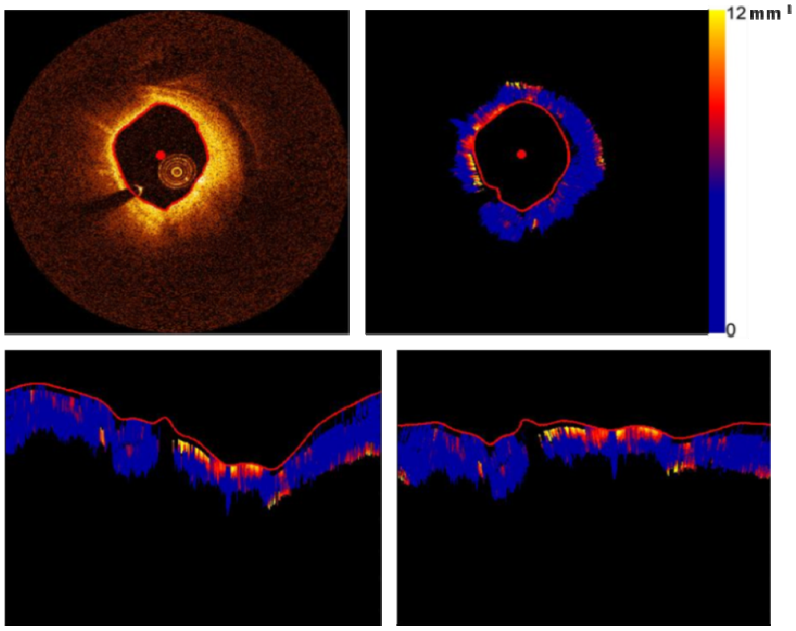

Fig. 2. Top left and right: OCT and attenuation images with lumen border and the centroid. Bottom left and right: Polar image before and after the shift of origin.

In the next step, we make a longitudinal attenuation map of the vessel. This mapping display of OCT attenuation depicts tissue optical properties in the entire pullback, sampling a user specified depth window from the lumen border, which at different conditions can be compared to quantify any difference. Such a map image is shown in Fig. 3.

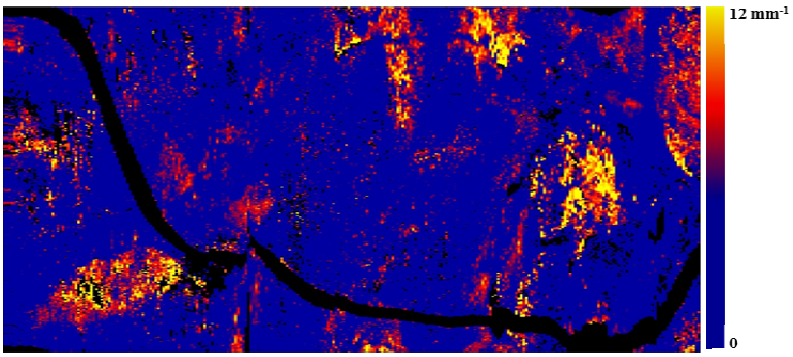

Fig. 3. Longitudinal attenuation map of a vessel sampled at a depth of 100-200 µm depicting the highly attenuating features in the entire pullback.

The attenuation map is made by taking the mean of 20 pixels from the depth of 100 µm from the lumen border (100-200 µm) along each A-line in all the frames across the pullback. The resulting longitudinal map has dimensions of frame number (x-axis), rotational angle (y-axis) and color codes the mean attenuation coefficient from 0 to 12 mm^{-1}. Such a map may highlight the lipid plaques and other high attenuating features in the entire pullback.

Even though the OCT pullbacks at different conditions are undertaken on the same vessel, it cannot be expected to exactly match due to factors such as non-uniform rotation, frame spacing and catheter orientation. To undertake quantitative comparison the attenuation map at different conditions should ideally be co-registered.

#202313 - $15.00 USD Received 5 Dec 2013; revised 24 Jan 2014; accepted 1 Feb 2014; published 3 Mar 2014

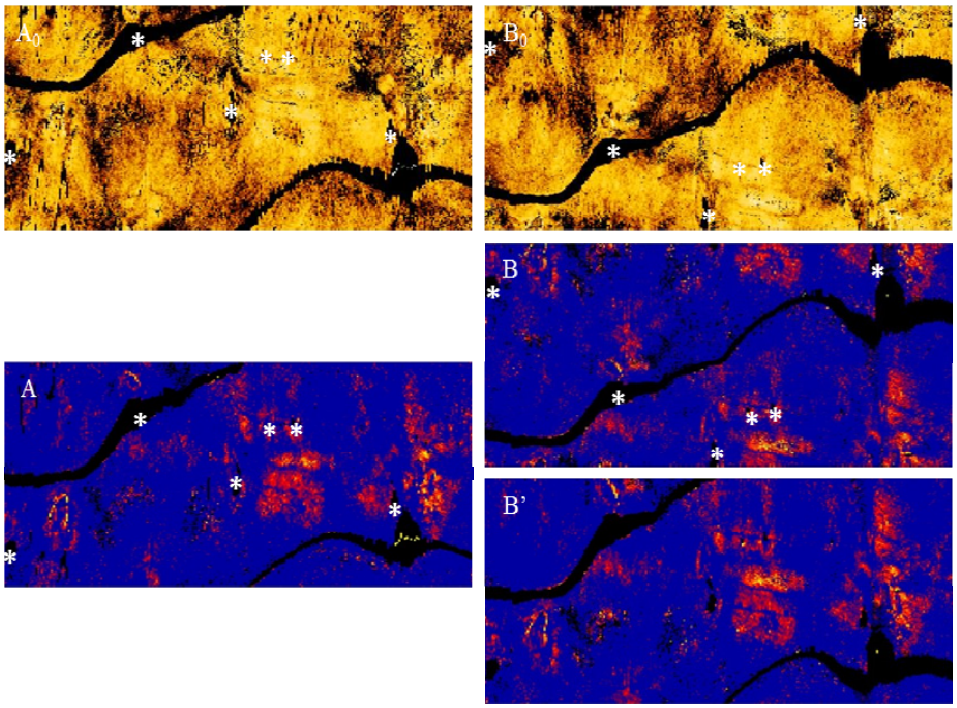

Fig. 4. Top: The en-face OCT map of pullbacks performed at UB (A_0) and FB (B_0) conditions; before registration. Bottom: The attenuation maps of the same pullbacks (A and B) where * indicates the control points used for registration, leading to (B'), the attenuation map after registration.

The registration procedure involves three steps. There is a first step of circularly shifting the images in the angular (y) direction. In the next step, an OCT intensity image map, folded out in the same manner as the attenuation data is used to select control points at side branches and other landmarks. A 2nd degree polynomial is fitted to the control points to derive a non-rigid transformation, which is then applied to the images. Finally, the data sets are cropped to represent the same physical length, as the pullback distal end can vary slightly and to avoid the guide catheter. Figure 4 shows an example of the unregistered OCT and attenuation maps with the control points and registered attenuation map images.

2.4 Image analysis

In order to establish the presence and possible magnitude of the differences between OCT data at different temperatures and fixation conditions, we analyzed the images qualitatively [11], assessing image appearance, and quantitatively, quantifying the difference in attenuation coefficient.

A quantitative comparison between the attenuation maps will be dominated by mismatched data if it depends on pixel-perfect alignment, even with the elaborate registration applied here. To avoid this pitfall, the registered images are processed in overlapping kernels of 60 × 15 pixels, with a step size of 15 pixels in the angular direction and 5 pixels in the longitudinal direction. We analyze the median value of the attenuation coefficient within this kernel size. Any difference between tissue optical attenuation in both conditions can be studied by analyzing a scatter plot of the median attenuation, comparing a modified condition to the the one that most accurately approximates in vivo circumstances (37°C, unfixed tissue). Differences in attenuation are quantified by finding the ratio of the median value of the kernels of other conditions against unfixed body temperature condition. We fit a line through the origin, the slope of which yields the root mean square difference. The size of the kernel is

#202313 - $15.00 USD Received 5 Dec 2013; revised 24 Jan 2014; accepted 1 Feb 2014; published 3 Mar 2014

determined by maximizing R^2 of this linear fit. The statistical evaluation of the data is completed by a Bland-Altman analysis.

A similar analysis as the one discussed above was performed on the OCT image intensity itself, to assess any effect of fixation or temperature on the backscatter coefficient μ_b, which is implicit in I_0 in (1) [15]. We studied the mean intensity at a depth of 100-200 μm from the lumen boundary, as shown in Fig. 4 (A_0 and B_0).

3. Results

3.1 Qualitative assessment

The potential similarities and differences of the parametric OCT images of tissues acquired under the different conditions are assessed qualitatively and quantitatively. Figure 5 illustrates a qualitative comparison of the cross-sectional OCT images before and after fixation matched with histology from that site in the vessel.

The histology shows a prominent streak of macrophages extending from the luminal surface into a fibro-lipidic plaque. The macrophage infiltration is evident in the OCT images pre- and post-fixation. In support of this observation, the corresponding attenuation images demonstrate a highly attenuating region consistent with macrophages [15, 29].

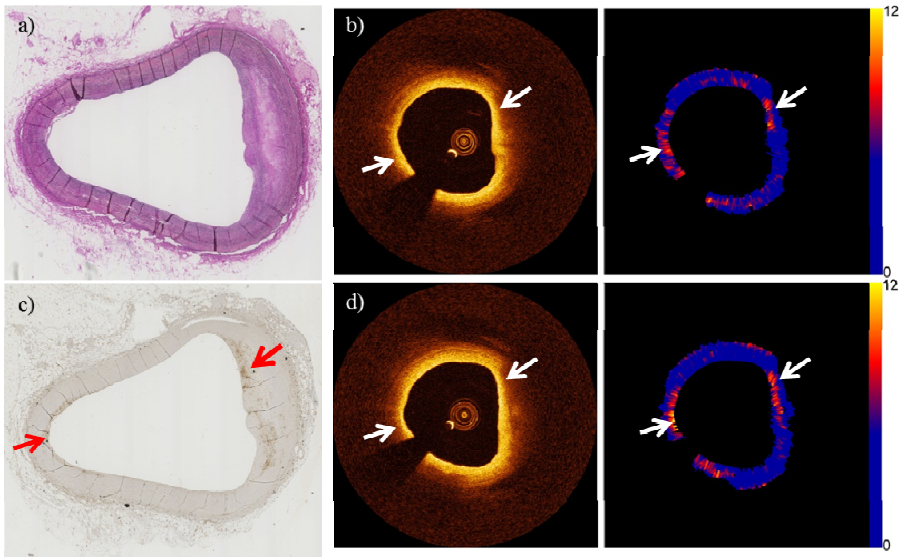

Fig. 5. (a) H&E and (c) CD68 stained histology image of a cross section. OCT and attenuation images of the cross section before (b) and after (d) fixation. The arrows indicate a streak of macrophages in the intima overlying a lipid pool. Additionally, luminal macrophage are evident on CD68 staining (arrowheads) with associated attenuation.

Qualitatively, no systematic differences were found between the data acquired before and after fixation, neither in the OCT images themselves, nor in the attenuation coefficients. We did observe variations in image intensity or attenuation, but these could be attributed to position mismatches in the undersampled pullbacks.

Likewise, we did not find any systematic difference between the OCT images of the same cross section acquired at different temperature conditions. Figure 6 shows the CD68 histology stain of a different cross section, compared to the OCT and attenuation images of the cross section in cold, room and body temperature conditions. The significant plaque feature in the cross section, the macrophages, are distinguishable at all temperature conditions. The attenuation values are comparable for all temperatures.

#202313 - $15.00 USD Received 5 Dec 2013; revised 24 Jan 2014; accepted 1 Feb 2014; published 3 Mar 2014

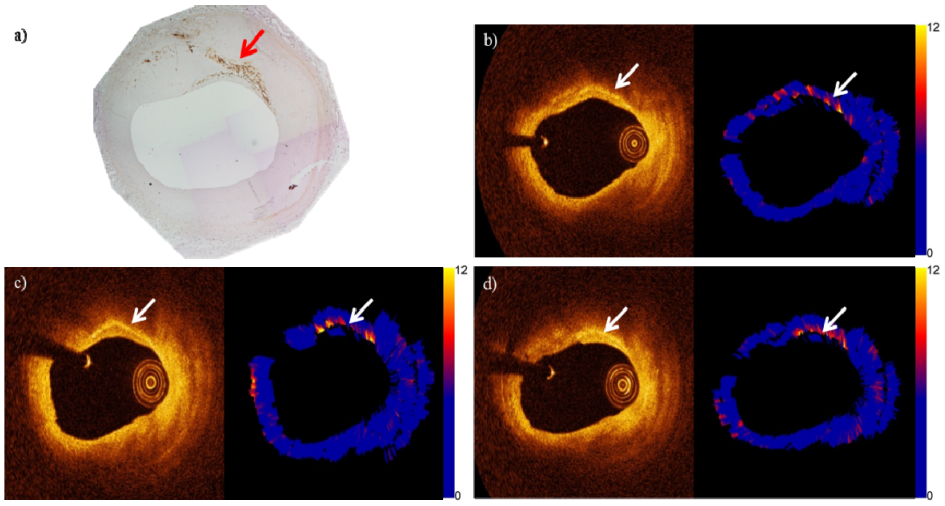

Fig. 6. (a) CD68 stained histology image of a cross section. The arrow indicate the streak of macrophages. OCT and attenuation images (in units of mm^{-1}) of the cross section in (b) UC, (c) UR and (d) UB conditions. The arrows indicate the streak of macrophages.

3.2 Quantitative assessment

The repeatability of OCT is well established but subject to effects including variation in pullback starting point, heart motion and more importantly the lumenal position of the catheter. Despite the use of our cadaveric heart rig and sequential imaging without removal of guidewire or imaging catheter, comparison of the OCT maps demonstrate variability preventing a pixel by pixel comparison. Consequently, comparison was limited to the median attenuation values in 60 x 15 pixel kernels in the longitudinal en-face map. The control condition for comparison is unfixed tissue at 37°C, considered to most closely match in-vivo conditions.

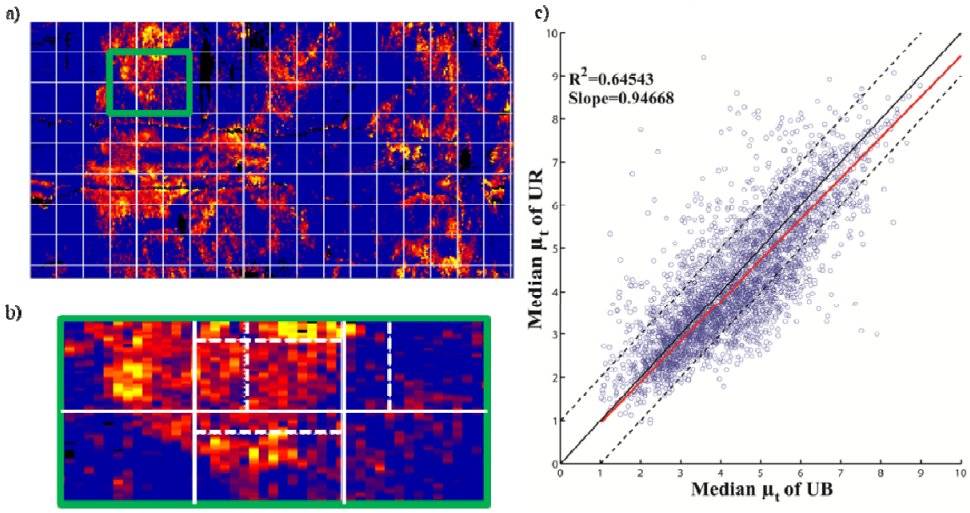

Fig. 7. (a) Attenuation map of a vessel with the considered kernels (b) the part of the map (in (a)) highlighted in green depicting the overlapping kernels (c) scatter plot of the medians of the kernels in UB and UR conditions with the fitted straight line through origin (red) and the line with slope 1 (black) and the lines with +/– 1 mm^{-1} (dotted).

#202313 - $15.00 USD Received 5 Dec 2013; revised 24 Jan 2014; accepted 1 Feb 2014; published 3 Mar 2014

When comparing the medians from all other conditions to control, ideally they should have identical values. So the reasonable quantities to be checked are the ratio of the median attenuation coefficient in matching regions in different conditions, and the slope of the line through the origin of the scatter plot of medians (the coefficient of proportionality).

Figures 7(a) and 7(b) show the attenuation map of fresh body temperature of a vessel with the considered kernals of 60 × 15 pixels and the moving kernel step size. Figure 7(c) depicts the scatter plot of the median of the kernels between the two conditions with the fitted line through the origin and the R^2 value.

Figure 8 shows the box plot of the ratio of the median attenuation values of all conditions against UB condition and the resulting coefficient of proportionality in each case.

Bland-Altman analysis produced mean differences close to zero for all comparisons (ranging from 0 to 0.2 mm^{-1}) and 95% confidence intervals between 0.5 and 1.5 mm^{-1}, which is consistent with the accuracy of the attenuation algorithm. No statistically significant trends were found.

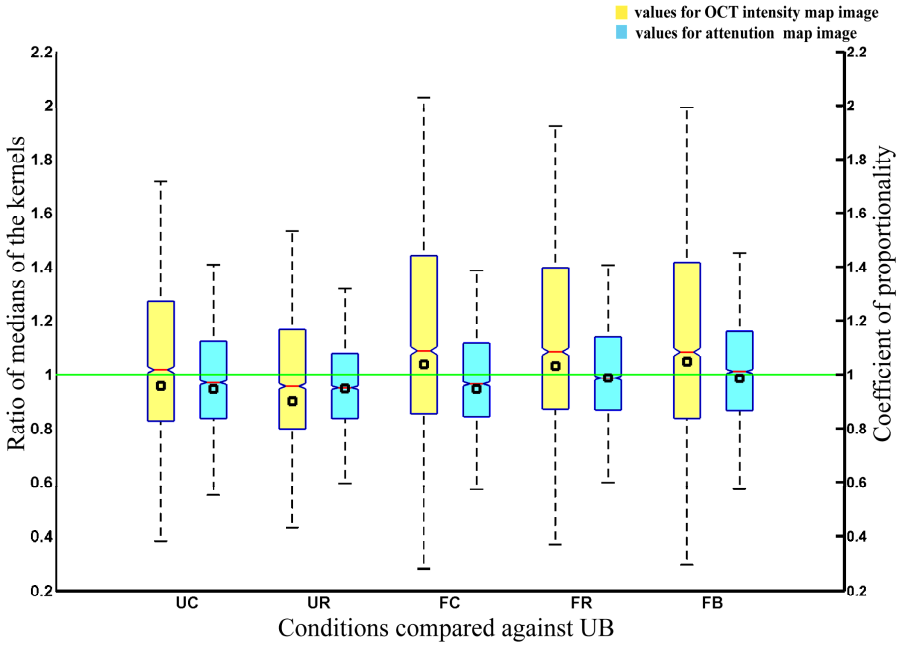

Fig. 8. (left y-axis) Box plot of the ratio of the median values of OCT intensity and attenuation in 60 x 15 kernels, plotted as median (red), 25th and 75th percentile (blue box), and 1.5 times the interquartile (whiskers). (right y-axis) Black squares: coefficient of proportionality extracted from the slope of the fit line for all the conditions.

In an analysis of the OCT image intensities, we found that the scatter in the data is much larger than for the attenuation coefficient, with typically $R^2 \approx 0.4$ for the linear fit and a median intensity ratio interquartile range of 0.6. One finding which appears to be robust, however, is that the image intensity is 11% higher in the OCT data of fixed tissue compared to unfixed, as measured by the ratio of the region medians as shown in Fig. 8.

4. Discussion

This study quantifies the effects of common tissue preparation steps on the optical properties of the artery wall. As new OCT analysis techniques are routinely developed on ex vivo tissues, it is important to know how temperature and tissue fixation affect the parameters that can be quantified from the OCT images. We extract the attenuation coefficient from the OCT images, a parameter that is relevant for tissue type. In our data, we see very small differences

#202313 - $15.00 USD Received 5 Dec 2013; revised 24 Jan 2014; accepted 1 Feb 2014; published 3 Mar 2014

induced by temperature and fixation: relative to unfixed tissue at 37°C, the attenuation coefficient differs by a few percent at most in other conditions.

We studied the ratios of median attenuation values in different conditions, and the coefficient of proportionality. The ratios are scattered in a narrow range around unity, while the coefficient of proportionality, which is more sensitive to outliers, is around 0.95. A 5% deviation converts to 0.5 mm^{-1} error on 10 mm^{-1} attenuation. We typically find that the attenuation of a single tissue type varies within a range larger than 0.5 mm^{-1}, so the variation in the condition is not resolvable. This result supports the main conclusion of this work: tissue attenuation in coronary arteries ex vivo can be studied in fixed tissues, without special precautions for temperature, which may greatly facilitate data collection. The image intensity itself does appear to be affected by fixation. In the absence of attenuation changes, this suggests that the scattering phase function is modified by the microstructural changes in the tissue, leading to a larger backscattering coefficient. This observation is consistent with our experience that OCT images in fixed tissues appear brighter than matched unfixed images.

We base our attenuation comparison partially on linear fits through the scatter plots of the median attenuation in different conditions. However, the influence of temperature and fixation on the optical properties of different tissues need not be the same, which potentially causes a regression to the mean. In general, a linear relationship cannot be expected between the maps of different conditions, but we did not find any evidence for deviations from simple proportionality. This finding is further supported by the absence of trends in the Bland-Altman analysis. We chose to minimize the number of degrees of freedom by fitting a line through the origin.

We compare the median, and not the mean, because it is less sensitive to skewed distributions of the attenuation values in a region of interest. Other signal or image statistics could be studied as well: it is conceivable that changes to the tissue microstructure caused by handling or preservation affect the intensity variation or the scattering phase function. Such changes could show up in higher order intensity statistics, or the backscatter coefficient, respectively. The latter is proving to be a parameter that is surprisingly resistant to quantitation. As we have demonstrated the relation between attenuation and tissue type [15], while other parameters are less studied, we chose to restrict the present study to attenuation only.

We have developed an analysis method that is robust against common registration errors. The OCT pullback has a large frame pitch relative to the width of the point spread function (the “frame thickness”) that can make it difficult to find the same cross section even in pullbacks of the same region of a vessel. Each frame of the OCT pullback is effectively made up of a spiral image of 200 μm through the vessel and therefore may not be accurately represented by a 3 μm thick histology section. This is essentially a sampling problem, that we deal with by constructing a longitudinal representation of the pullback to make quantitative comparisons. This has several advantages over analysis in cross section images. A longitudinal map brings out tissue features as a whole, along the vessel, while in a cross section only a part of it can be located. It also allows for non-rigid registration to correct for non-uniform rotation and variations in effective pullback speed (due to cardiac motion in vivo). The longitudinal representation remains a two-dimensional cross section through a three-dimensional data set, and sacrifices depth resolution. For detailed analyses, several longitudinal maps at different depths from the lumen boundary can be extracted. In order to eliminate sensitivity of the comparison to pixel-perfect alignment, we studied the median values of kernels of 60 × 15 pixels. This is necessary to extract meaningful differences, as any parametric difference between the various conditions would be obscured by large differences introduced by mismatches. The size of the kernel 60 × 15 pixels was chosen by maximizing the R^2 values of the fit.

The accuracy of the non-rigid registration step depends on the number of landmarks that are usable as control points. We attribute the remaining scatter in the data sets to persisting

#202313 - $15.00 USD Received 5 Dec 2013; revised 24 Jan 2014; accepted 1 Feb 2014; published 3 Mar 2014

registration errors. These introduce a variance that is not explained by the analysis model and affect the R^2 of the fit for the medians. We find $R^2 \approx 0.6$, which still represents significant accuracy of the fit.

4.1 Study limitations

Co-registration of multiple OCT images acquired at varying conditions, and comparison against histology is challenging. Despite careful reproduction of OCT imaging at all conditions and computational co-registration we concede that exact matching of images is not possible. However, we believe our methods of matching generate accurate comparisons. The inherent differences in longitudinal resolution between OCT (200um) & histology (3um) highlight OCT's tendency to under-sample the vessel. We have overcome this by undertaking extensive histological preparation of vessel segments containing plaque of interest, allowing 'best-fit' matching with the lower resolution OCT images. Maintenance of steady-state temperature in the cadaveric heart model required prolonged infusion of PBS, incubated to the selected condition temperature. Despite measurement of vessel temperature with a needle-probe thermometer, it is possible that a temperature gradient existed from the vessel lumen into deeper tissue but not expected to be very significant considering the penetration depth of the OCT. The ultimate aim of this work is to facilitate translation into the clinical setting; however, we must concede that despite evaluation of variations in attenuation generated by temperature and fixation, other significant differences exist between the ex-vivo & in-vivo environment. Particularly, the influence of cardiac motion on image acquisition and the potential influence of luminal blood on image quality.

5. Conclusion

The results show that the ratio of the median attenuation values of kernels and the coefficient of proportionality or the slope of the line through the origin fitted for the medians is close to unity for every condition against the base condition. The largest deviation in slope from one is 0.06, leading to a change in tissue attenuation of less than 1 mm^{-1}, which is the approximate accuracy of the algorithm. The results suggest that fixation and room temperature conditions in the ex-vivo OCT experiments do not induce a systematic error.

Acknowledgments

This work was funded by the Netherlands Heart Foundation grant (2010B064) and Heart Research UK (RG2608/12/14) and supported by researchers at the National Institute for Health Research Bristol Cardiovascular Biomedical Research Unit. We thank Pieter Kruizinga and Takeyoshi Kameyama for providing insight and expertise that greatly assisted the research and Jolanda Wentzel for helpful discussion. We also thank Mr. Paul Chappell of the workshop in BHI.